METROLOGY

Measurement of the fine-structure constant as a test of the Standard Model

Richard H. Parker,[1]* Chenghui Yu,[1]* Weicheng Zhong,[1] Brian Estey,[1] Holger Müller[1,2]†

Measurements of the fine-structure constant α require methods from across subfields and are thus powerful tests of the consistency of theory and experiment in physics. Using the recoil frequency of cesium-133 atoms in a matter-wave interferometer, we recorded the most accurate measurement of the fine-structure constant to date: α = 1/137.035999046(27) at 2.0 × 10^{-10} accuracy. Using multiphoton interactions (Bragg diffraction and Bloch oscillations), we demonstrate the largest phase (12 million radians) of any Ramsey-Bordé interferometer and control systematic effects at a level of 0.12 part per billion. Comparison with Penning trap measurements of the electron gyromagnetic anomaly g_e − 2 via the Standard Model of particle physics is now limited by the uncertainty in g_e − 2; a 2.5σ tension rejects dark photons as the reason for the unexplained part of the muon's magnetic moment at a 99% confidence level. Implications for dark-sector candidates and electron substructure may be a sign of physics beyond the Standard Model that warrants further investigation.

The fine-structure constant α characterizes the strength of the electromagnetic interaction between elementary charged particles. It has been measured by various methods from diverse fields of physics (Fig. 1), and the agreement of these results confirms the consistency of theory and experiment across fields. In particular, α can be obtained from measurements of the electron's gyromagnetic anomaly g_e − 2 by using the Standard Model of particle physics, including quantum electrodynamics to the fifth order (involving >10,000 Feynman diagrams) and muonic as well as hadronic physics (*1*–*3*). This path leads to an accuracy of 0.24 part per billion (ppb) (*4*–*6*) and was until now the most accurate measurement of α.

An independent measurement of α at comparable accuracy creates an opportunity to test the Standard Model. The most accurate of previous such measurements have been based on the kinetic energy $\hbar^2k^2/(2m_{At})$ of an atom of mass m_{At} that recoils from scattering a photon of momentum $\hbar k$ (*3*), where $\hbar$ is Planck's constant h divided by 2π, and $k = 2\pi/\lambda$ is the laser wave number (where λ is the laser wavelength). Experiments of this type yield h/m_{At} and have measured α to 0.62 ppb (*7*) via the relation

$$\alpha^2 = \frac{2R_\infty}{c}\frac{m_{At}}{m_e}\frac{h}{m_{At}}$$

The Rydberg constant R_∞ is known to 0.006-ppb accuracy (*6*), and the atom-to-electron mass ratio $\left(\frac{m_{At}}{m_e}\right)$ is known to better than 0.1 ppb for many species. Here, c represents the speed of light in vacuum.

The fundamental tool of our experiment is a matter-wave interferometer (*8*, *9*). Similar to an optical interferometer, this apparatus splits waves from a coherent source along different paths, recombines them, and measures the resulting interference to extract the phase difference accumulated between the waves on the paths. Sequences of laser pulses are used to direct and recombine the atomic matter waves along different trajectories, to form a closed interferometer (*10*). The phase evolution is governed by the Compton frequency of the atoms. The probability of detecting each atom at the output of the interferometers is a function of the phase accumulated between the different paths; measurement of the total atom population in each output enables an estimate of this phase. For the Ramsey-Bordé interferometer geometry used in this experiment, the phase is proportional to the photon recoil energy and can therefore be used to measure the ratio h/m_{Cs} (m_{Cs}, mass of a cesium atom) and, from that, the fine-structure constant α.

In our experiment, we used a number of methods to increase the signal and suppress systematic errors. We used 10-photon processes as beam

[1]Department of Physics, 366 Le Conte Hall MC 7300, University of California, Berkeley, CA 94720, USA. [2]Lawrence Berkeley National Laboratory, One Cyclotron Road, Berkeley, CA 94720, USA.
*These authors contributed equally to this work.
†Corresponding author. Email: hm@berkeley.edu

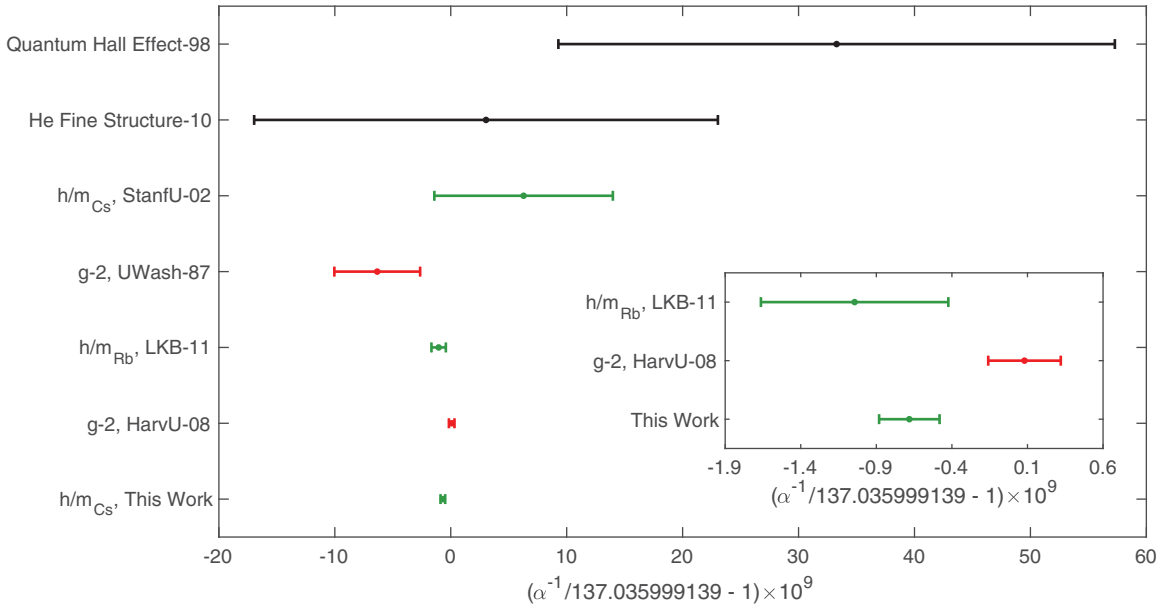

Fig. 1. Precision measurements of the fine-structure constant. A comparison of measurements (*1*, *3*–*5*, *7*, *26*–*28*). "0" on the plot is the CODATA 2014 recommended value (*7*). The green points are from photon recoil experiments; the red ones are from electron g_e − 2 measurements. The inset is a close-up view of the bottom three measurements. Error bars indicate 1σ uncertainty. StanfU, Stanford University; UWash, University of Washington; LKB, Laboratoire Kastler Brossel; HarvU, Harvard University.

splitters for the matter waves; these processes increase the recoil energy by a factor of 25 relative to standard two-photon Raman processes (*11*). To accelerate the atoms by up to another 800$\hbar k$ (400$\hbar k$ up, 400$\hbar k$ down), we applied a matter-wave accelerator: Atoms were loaded into an optical lattice, a standing wave generated by two laser beams, which was accelerated by ramping the frequency of the lasers (Bloch oscillations) (*7*, *12*). Coriolis force compensation suppressed the effect of Earth's rotation. In addition, we applied ac Stark shift compensation (*13*, *14*) and demonstrated a spatial-filtering technique to reduce sources of decoherence, further enhance the sensitivity, and suppress systematic phase shifts. An end-to-end simulation of the experiment was run (*12*) to help us identify and reduce systematic errors and confirm the error budget. To avoid possible bias, we adopted a blind measurement protocol, which was unblinded only at the end. Combining with precise measurements of the cesium (*15*) and electron (*16*) mass, we found

$$\alpha^{-1} = 137.035999046(27)$$

with a statistical uncertainty of 0.16 ppb and a systematic uncertainty of 0.12 ppb (0.20 ppb total). Our result is a more than threefold improvement over previous direct measurements of α (*7*). The measurement of h/m_{Cs} = 3.0023694721 (12) × 10^{-9} m^2/s also provides an absolute mass standard in the context of the proposed new definition of the kilogram (*10*). This proposed definition will assign a fixed numerical value to Planck's constant, to which mass measurements could then be linked through measurements of h/m_{At}, such as this one, via Avogadro spheres. Our result agrees with previous recoil measurements (*7*) within 1σ uncertainty and has a 2.5σ tension with measurements (*4*–*6*) based on the gyromagnetic moment.

Table 1. Error budget. For each systematic effect, more discussion can be found in the listed section of the supplementary materials. N/A, not applicable.

Effect	Section	δα/α (ppb)
This study		
Laser frequency	1	−0.24 ± 0.03
Acceleration gradient	4A	−1.79 ± 0.02
Gouy phase	3	−2.60 ± 0.03
Beam alignment	5	0.05 ± 0.03
Bloch oscillation light shift	6	0 ± 0.002
Density shift	7	0 ± 0.003
Index of refraction	8	0 ± 0.03
Speckle phase shift	4B	0 ± 0.04
Sagnac effect	9	0 ± 0.001
Modulation frequency wave number	10	0 ± 0.001
Thermal motion of atoms	11	0 ± 0.08
Non-Gaussian waveform	13	0 ± 0.03
Parasitic interferometers	14	0 ± 0.03
Total systematic error	All previous	−4.58 ± 0.12
Statistical error	N/A	±0.16
Other studies		
Electron mass (*16*)	N/A	±0.02
Cesium mass (*6*, *15*)	N/A	±0.03
Rydberg constant (*6*)	N/A	±0.003
Combined result		
Total uncertainty in α	N/A	±0.20

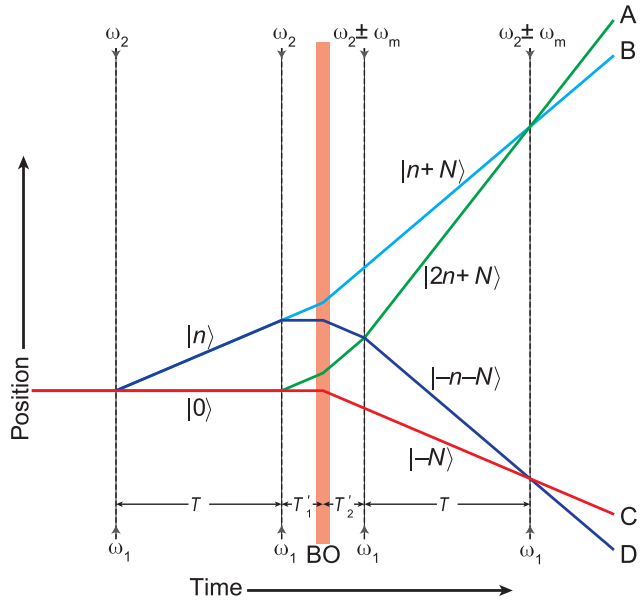

Fig. 2. Simultaneous conjugate atom interferometers. Solid lines denote the atoms' trajectories; dashed lines represent laser pulses with their frequencies indicated. $|n\rangle$ denotes a momentum eigenstate with momentum $2n\hbar k$. BO, Bloch oscillations. In this figure, gravity is neglected. A to D represent interferometer outputs.

Our matter-wave interferometer is based on the one described in (*12*), in which cesium atoms are loaded in a magneto-optical trap, launched upward in an atomic fountain, and detected as they fall back down—the interferometer sequence occurs during the parabolic flight. Figure 2 shows the trajectories of an atom wave packet in our experiment, formed by impulses from pairs of vertical, counterpropagating laser pulses on the atoms. Each pulse transfers the momentum of $2n$ = 10 photons (where n is the order of Bragg diffraction) with near 50% probability by multiphoton Bragg diffraction, acting as a beam splitter for matter waves. Bragg diffraction allows for large momentum transfer at each beam splitter, creating a pair of atom wave packets that separate with a velocity of ~35 mm/s. After a time interval T, a similar pulse splits the wave packets again, creating one pair that moves upward and one that moves down.

The third and fourth pulses recombine the respective paths to form two interferometers. Between the second and the third pulses, we accelerated the atom groups further from one another, using Bloch oscillations in accelerated optical lattices, to increase the sensitivity and suppress systematic effects. This transfers $+2N\hbar k$ of momentum to the upper interferometer and $-2N\hbar k$ to the lower interferometer (N, number of Bloch oscillations) (*13*).

The phase difference between the interferometer arms arises as a result of the kinetic energy $(\hbar k)^2/(2m_{Cs})$ that the atoms gain from the recoil momentum of the photon-atom interactions and from the phase transferred during the atoms' interaction with the laser beams. Taking the phase difference between the two interferometers cancels effects due to gravity and vibrations. In the absence of systematic effects, the overall phase Φ of the interferometer geometry shown in Fig. 2 is given by (*12*, *17*)

$$\Phi = \Delta\phi_1 - \Delta\phi_2 = 16n(n+N)\omega_r T - 2n\omega_m T$$

where $\Delta\phi_{1,2}$ are the measured phases of the two interferometers individually, $\omega_r = \hbar k^2/(2m_{Cs})$ is the photon recoil frequency, T is the time between the laser pulses, and ω_m is the laser frequency difference we choose to apply between

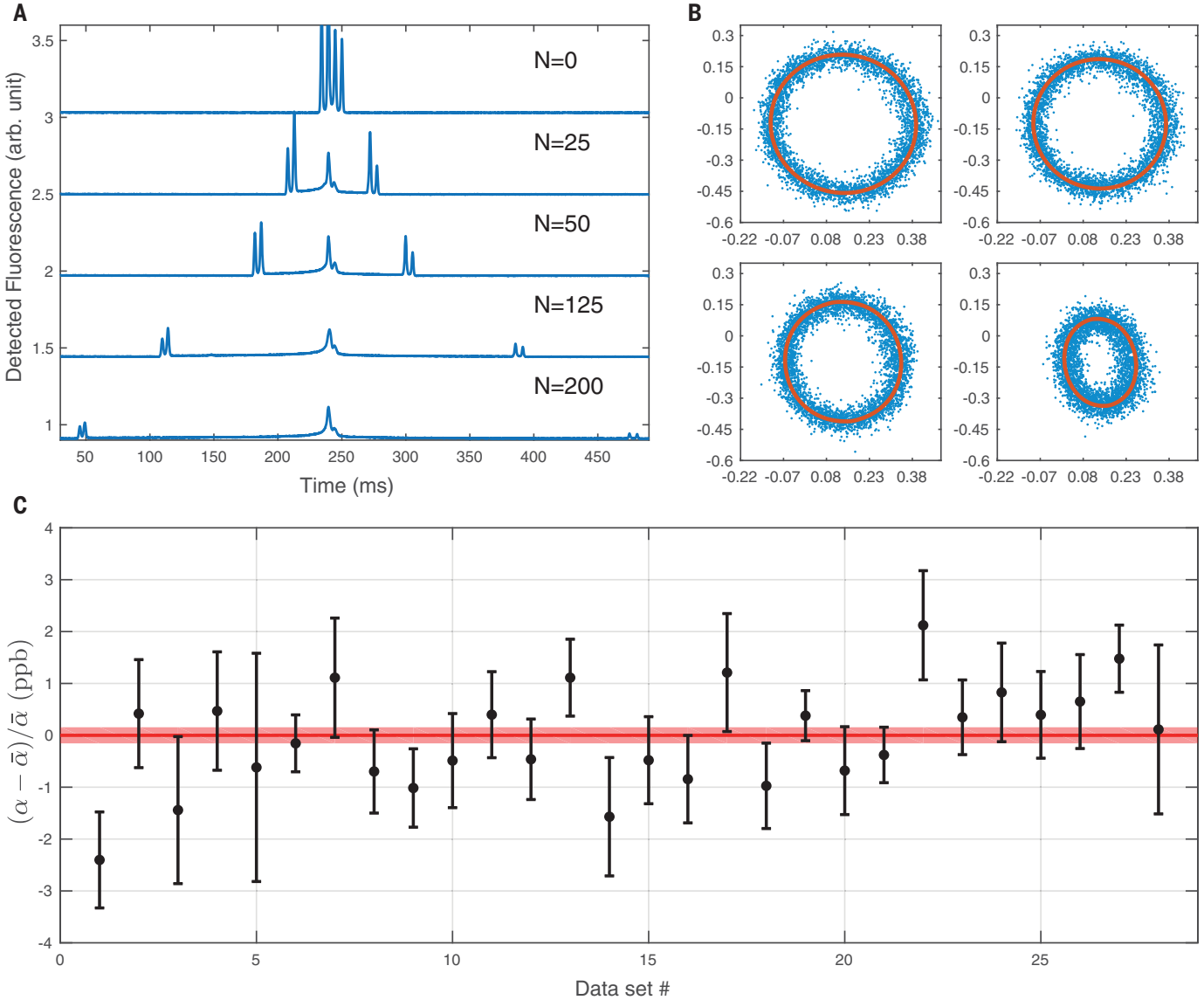

Fig. 3. Data analysis. (**A**) Fluorescence signals of the atom clouds as they fall through the detection region, after the interferometer sequence, for varying number N of Bloch oscillations, measured with fixed laser power and acceleration of the atoms during Bloch oscillations. For visibility, a vertical offset has been applied to each trace. The four outer peaks correspond to the four outputs A to D (Fig. 2) of the interferometers. Atoms left behind by the Bloch oscillations form the central peaks; they do not contribute to the measurement. T = 5 ms for these data sets. (**B**) Outputs of each interferometer are normalized and plotted parametrically: the x axis is (C − D)/(C + D) and the y axis is (A − B)/(A + B) (A to D are defined in Fig. 2). This produces an ellipse, which is fitted to extract the differential phase. The ellipses shown are for n = 5, N = 125, and T = 5, 20, 40, and 80 ms (for a total interferometer phase of >10 Mrad), respectively. (**C**) Data sets used in the determination of α. The pink band represents the overall ±1σ statistical error. The reduced χ^2 for the combined data is 1.2, with a P value of 0.2. $\bar{\alpha}$ is the weighted average of the measurements. Error bars indicate 1σ uncertainty.

the first and second pairs of pulses (Fig. 2). A measurement proceeds by adjusting ω_m to find the point where $\Phi = 0$ so that $\omega_m = 8(n + N)\omega_r$. Because the wave number k of the laser is related to the laser frequency, this yields h/m_{Cs} and, thus, α. In our measurement, n = 5, N = 125 to 200, and T = 5 to 80 ms, so that Φ is 10^6 to 10^7 rad and ω_m is 2 to 3 MHz.

Our error budget (Table 1) includes the systematic effects considered in the previous rubidium h/m_{Cs} measurement (*7*). These systematic effects are dominant, and several methods are used to reduce them (*18*). Our laser frequency is monitored using a frequency comb generator. Effects caused by the finite radius of the laser beam are controlled by a retro-reflection geometry: delivering all components of the beam via the same single-mode optical fiber, using an apodizing filter to improve the Gaussian beam shape, selecting only atoms that stay close to the beam axis, and correcting for drift of the beam alignment in real time to further suppress such effects. The gravity gradient has been measured in situ for subtraction by configuring the atom interferometer as a gravity gradiometer (*19*–*21*). Keeping atoms in the same internal state while in all interferometer arms reduces the influence of the Zeeman effect to the one of an acceleration gradient, taken out by the gravity gradient measurement. The index of refraction and atom-atom interactions are reduced by the low density of our atomic sample (*18*).

New systematic effects arise from Bragg diffraction but can be suppressed to levels much smaller than the well-known systematics just mentioned. The potentially largest systematic is the diffraction phase Φ_0, which we have studied in previous work (*12*, *13*). It is caused primarily by off-resonant Bragg scattering in the third and fourth laser pulse,

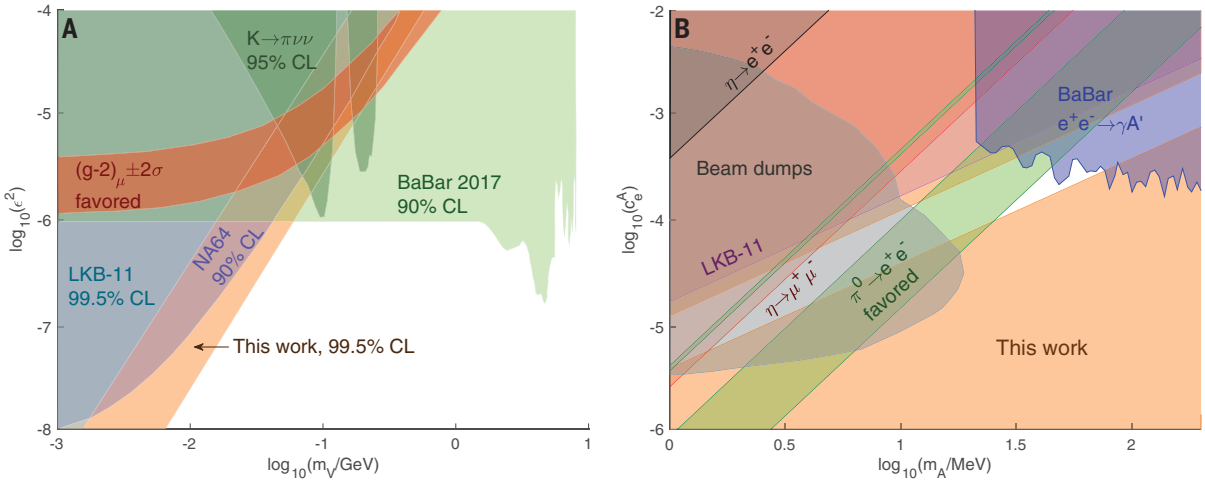

Fig. 4. Limits on dark bosons. (**A**) Excluded parameter space for dark photons (vector bosons), as a function of the dark-photon mass m_V and coupling suppressed by the factor ϵ. The shaded orange and blue regions are ruled out at the indicated CLs by comparing the measured a_e (*4*–*6*) with that predicted by our α measurement and the LKB-11 result, respectively (significance levels have been calculated for a one-tailed test). The red band denotes a 95% CL in which the muon $g_\mu - 2$ is explained by a dark photon. Because our measured δa is negative, our measurement disfavors dark photons. Accelerator limits are adapted from (*29*). (**B**) Excluded parameter space for dark axial vector bosons, as a function of mass m_A and axial-vector coupling constant c_A, whose existence would produce a negative δa and is thus favored. Our work results in a two-sided bound. The region suggested by anomalous pion decay is shown in green (*24*) at 95% CL. Accelerator limits are adapted from (*29*).

where multiple frequencies for the Bragg beams are used to simultaneously address both interferometers (Fig. 2). We can therefore suppress it by using a large number N of Bloch oscillations; this increases the velocity of the atoms and thus the Doppler effect, moving the off-resonant component further off resonance. It also increases the total phase, further reducing the relative size of the systematic. The diffraction phase is nearly independent of the pulse-separation time T, so we alternate between two or more (usually six) pulse-separation times and extrapolate $T \to \infty$.

To determine the residual T-dependent diffraction phase, we employed a Monte Carlo simulation and numerically propagated atoms through the interferometer (*13*, *18*). We ran the experiment at several different pulse-separation times, ensuring that there was no statistically significant signal for any unaccounted systematic variation. Overall, systematic errors contribute an uncertainty of 0.12 ppb to the measurement of α. As described in the supplementary materials, we corrected for systematic effects due to spatial intensity noise that have recently been pointed out (*22*) and for systematic effects due to deviations of the beam shape from a perfect Gaussian (*18*).

Figure 3C shows our data, which were collected over the course of 7 months. Each point represents roughly 1 day of data. The signal-to-noise ratio of our experiment would allow reaching a 0.2-ppb precision in less than 1 day, but extensive data were collected to suppress and control systematic effects. The measurement campaigns were interspersed with additional checks for systematic errors. Data sets typically include six different pulse-separation times, but nine data sets include only three different pulse-separation times and four data sets include four different pulse-separation times, repeated in ~15-min bins; the fit algorithm allows each bin of data to have a different diffraction phase (as the various experimental parameters may drift slowly over time) but assumes one value of h/m_{Cs} for the entire data set.

By combining our measurement with theory (*5*, *6*), we calculated the Standard Model prediction for the anomalous magnetic moment of the electron as

$$a(\alpha) = \frac{g_e}{2} - 1 = 0.00115965218161(23)$$

Comparison with the value obtained through direct measurement (a_{meas}) (*4*) yielded a negative $\delta a = a_{meas} - a(\alpha) = -0.88(0.36) \times 10^{-12}$. Comparison of our result to previous measurements of α (Fig. 1) produced an error bar below the magnitude of the fifth-order quantum electrodynamics calculations used in the extraction of α from the electron $g_e - 2$ measurement and thus allows us to confront these calculations with experiment.

In addition, our measurement can be used to probe a possible substructure within the electron. An electron whose constituents have mass $m* \gg m_e$ would result in a modification of the electron magnetic momentum by $\delta a \sim m_e/m*$. In a chirally invariant model, the modification scales as $\delta a \sim (m_e/m*)^2$. Following the treatment in (*23*), the comparison $|\delta a|$ of this measurement of α with the electron $g_e - 2$ result places a limit to a substructure at a scale of $m* > 411{,}000\ \mathrm{TeV}/c^2$ for the simple model and $m* > 460\ \mathrm{GeV}/c^2$ for the chirally invariant model (improvements over the previous limits of $m* > 240{,}000\ \mathrm{TeV}/c^2$ and $m* > 350\ \mathrm{GeV}/c^2$, respectively).

Precision measurements, such as ours, of α can also aid in the search for new dark-sector (or hidden-sector) particles (*18*). A hypothetical dark photon, which is parameterized by a mixing strength ϵ and a nonzero mass m_V, for example, would lead to a nonzero δa that is a function of ϵ and m_V (*24*). We can test the existence of dark photons by comparing our data with the electron $g_e - 2$ measurement (*4*). The blue area in Fig. 4A shows the parameter space that is inconsistent with our data. We note that dark photons cause a $\delta a > 0$, opposite to the sign measured in both our experiment and the rubidium measurement (*7*). With the improved error of our measurement, this tension has grown. A model consisting of the Standard Model and dark photons of any m_V or ϵ is now incompatible with the data at up to a 99% confidence level (CL). Constraints on the theory obtained in this fashion (Fig. 4A) include regions not previously bounded by accelerator experiments and do not depend on the assumed decay branching ratios of the dark photon.

By contrast, a dark axial vector boson characterized by an axial vector coupling c_A and mass m_A is favored by the data because it would lead to a negative δa, but we emphasize that the 2.5σ tension in the data is insufficient to conclude the existence of a new particle (Fig. 4B). The discrepancy between the two methods of measuring α could be a hint of possible physics beyond the Standard Model that warrants further investigation. The calculated δa places limits on the axial vector parameter space from two sides. The allowed region is partially ruled out by other experiments. However, the region of parameter space consistent with our result and anomalous pion decay is also consistent with current accelerator limits, and thus the remaining region of parameter space warrants further study (*24*).

In particular, dark photons are one proposed explanation for the 3.4σ discrepancy in the muon

$g_\mu - 2$ with respect to the Standard Model prediction (*25*). As shown in Fig. 4, we rule out this explanation for nearly all values of m_V and ϵ, rejecting dark photons as an explanation for the discrepancy at the 99% CL for any dark-photon mass. The comparison of precision measurements of α and $g_e - 2$ embodies a broad probe for new physics and enables us to search for (or exclude) a plethora of other previously unidentified particles that have been proposed, such as *B-L* vector bosons, axial vector–coupled bosons, and scalar and pseudoscalar bosons including those that mix with the Higgs field, such as the relaxion.

REFERENCES AND NOTES

1. T. Aoyama, M. Hayakawa, T. Kinoshita, M. Nio, *Phys. Rev. Lett.* **109**, 111807 (2012).
2. S. Laporta, *Phys. Lett. B* **772**, 232–238 (2017).
3. A. Wicht, J. M. Hensley, E. Sarajlic, S. Chu, *Phys. Scr. T* **2002**, 82 (2002).
4. D. Hanneke, S. Fogwell, G. Gabrielse, *Phys. Rev. Lett.* **100**, 120801 (2008).
5. T. Aoyama, M. Hayakawa, T. Kinoshita, M. Nio, *Phys. Rev. D* **96**, 019901 (2017).
6. P. J. Mohr, D. B. Newell, B. N. Taylor, *Rev. Mod. Phys.* **88**, 035009 (2016).
7. R. Bouchendira, P. Cladé, S. Guellati-Khélifa, F. Nez, F. Biraben, *Phys. Rev. Lett.* **106**, 080801 (2011).
8. A. D. Cronin, J. Schmiedmeyer, D. E. Pritchard, *Rev. Mod. Phys.* **81**, 1051–1129 (2009).
9. G. M. Tino, M. A. Kasevich, Eds., *Atom Interferometry* (Proceedings of the International School of Physics "Enrico Fermi," Course CLXXXVIII, Societa Italiana di Fisica and IOS Press, 2014).
10. S.-Y. Lan *et al.*, *Science* **339**, 554–557 (2013).
11. H. Müller, S. W. Chiow, Q. Long, S. Herrmann, S. Chu, *Phys. Rev. Lett.* **100**, 180405 (2008).
12. B. Estey, C. Yu, H. Müller, P.-C. Kuan, S.-Y. Lan, *Phys. Rev. Lett.* **115**, 083002 (2015).
13. R. H. Parker *et al.*, *Phys. Rev. A* **94**, 053618 (2016).
14. T. Kovachy *et al.*, *Nature* **528**, 530–533 (2015).
15. G. Audi *et al.*, *Chin. Phys. C* **36**, 1157 (2012).
16. S. Sturm *et al.*, *Nature* **506**, 467–470 (2014).
17. G. T. Foster, J. B. Fixler, J. M. McGuirk, M. A. Kasevich, *Opt. Lett.* **27**, 951–953 (2002).
18. See supplementary materials.
19. P. Asenbaum *et al.*, *Phys. Rev. Lett.* **118**, 183602 (2017).
20. F. Sorrentino *et al.*, *Phys. Rev. A* **89**, 023607 (2014).
21. G. Rosi *et al.*, *Phys. Rev. Lett.* **114**, 013001 (2015).
22. S. Bade, L. Djadaojee, M. Andia, P. Cladé, S. Guellati-Khélifa, arXiv:1712.04023 [physics.atom-ph] (11 December 2017).
23. G. Gabrielse, S. F. Hoogerheide, J. Dorr, E. Novitski, in *Fundamental Physics in Particle Traps*, W. Quint, M. Vogel, Eds. (Springer Tracts in Modern Physics Series, Springer, 2014), vol. 256.
24. Y. Kahn, G. Krnjaic, S. Mishra-Sharma, T. M. P. Tait, *J. High Energy Phys.* **2017**, 2 (2017).
25. F. Terranova, G. M. Tino, *Phys. Rev. A* **89**, 052118 (2014).
26. A. Jeffery *et al.*, *Metrologia* **35**, 83–96 (1998).
27. A.-M. Jeffery, R. E. Elmquist, L. H. Lee, J. Q. Shields, R. F. Dziuba, *IEEE Trans. Instrum. Meas.* **46**, 264–268 (1997).
28. M. Smiciklas, D. Shiner, *Phys. Rev. Lett.* **105**, 123001 (2010).
29. J. P. Lees *et al.*, *Phys. Rev. Lett.* **119**, 131804 (2017).

ACKNOWLEDGMENTS

We acknowledge helpful discussions with O. Schwartz, P. Hamilton, M. Pospelov, S. Chu, B. Taylor, P.-C. Kuan, S.-Y. Lan, T. Tait, and E. Copenhaver. We thank R. Adhikari for being the "keeper" of the random number used in the blind analysis. We are particularly grateful to S. Guellati-Khélifa and P. Cladé for bringing to our attention the change in effective Gouy phase due to intensity variations on the beam. **Funding:** This work was supported by the Alfred P. Sloan Foundation (grant BR-5044), the David and Lucile Packard Foundation (grant 2009-34712), Jet Propulsion Laboratory (grants 1458850, 1483242, 1531033, and 1553641), National Institute of Standards and Technology (award 60NANB9D9169), NSF (CAREER award PHY-1056620 and MRI award PHY-0923445), and the University of California Office of the President (award 040219). **Author contributions:** All authors contributed jointly to all aspects of this work. **Competing interests:** The authors declare no competing interests. **Data and materials availability:** All data needed to evaluate the conclusions in the paper are present in this paper and the supplementary materials.

SUPPLEMENTARY MATERIALS

www.sciencemag.org/content/360/6385/191/suppl/DC1
Supplementary Text
Figs. S1 to S10
Table S1
Reference (*30*)

24 August 2017; accepted 21 February 2018
10.1126/science.aap7706

Measurement of the fine-structure constant as a test of the Standard Model

Richard H. Parker, Chenghui Yu, Weicheng Zhong, Brian Estey and Holger Müller

Science **360** (6385), 191-195.
DOI: 10.1126/science.aap7706

Refining the fine-structure constant

The fine-structure constant, α, is a dimensionless constant that characterizes the strength of the electromagnetic interaction between charged elementary particles. Related by four fundamental constants, a precise determination of α allows for a test of the Standard Model of particle physics. Parker *et al.* used matter-wave interferometry with a cloud of cesium atoms to make the most accurate measurement of α to date. Determining the value of α to an accuracy of better than 1 part per billion provides an independent method for testing the accuracy of quantum electrodynamics and the Standard Model. It may also enable searches of the so-called "dark sector" for explanations of dark matter.

Science, this issue p. 191